Journal of Biosensors & Bioelectronics
ISSN: 2155-6210

Yuan, J Biosens Bioelectron 2013, 4:3
DOI: 10.4172/2155-6210.1000135

Research Article Open Access

Model-Based Quantification of Blood Flow Rate and Oxygen Consumption Rate of Biological Tissues Using Image-Guided Near Infrared Light Spectroscopy

Zhen Yuan*

Faculty of Health Sciences, University of Macau, Av. Padre Tomás Pereira, Taipa, Macau, China

Abstract

Image-guided near infrared spectroscopy has been implemented to deduce the map of oxygen consumption rate and blood flow rate of biological tissues using a model-based method combined the noninvasive diffuse light measurement techniques. The developed method relies on optical imaging to recover the concentrations of oxygen and de-oxygen hemoglobin concentration of tissues, and the ordinary differential equations to recover the vascular parameters including oxygen consumption rate and blood flow rate. In particular, the mathematical model has been validated by both simulation and experimental tests.

Introduction

Analysis of the physiological responses of functional brain activation based on intrinsic optical signals has revealed new insights into the functional representations of areas such as the visual and somatosensory cortices [1,2]. In addition to hemoglobin change, cerebral blood flow rate (*CBF*) and oxygen consumption rate (*OC*) changes resulting from functional activation are also important components of the hemodynamic response. The nature of the coupling between neuronal activity and the associated hemodynamic response is now becoming an interesting subject in neuroscience [3,4]. Clearer understandings of the neuro-metabolic-vascular relationship will enable greater insight into the functioning of the normal brain and will also have significant impact on diagnosis and treatment of neurovascular diseases such as stroke, Alzheimer's disease, and head injury and epilepsy [5]. In order to achieve this goal, simultaneous monitoring of the spatiotemporal characteristics of *OC, CBF*, and the cerebral metabolic rate of oxygen is crucial.

Although many methods for assessment of cerebral *OC* and *CBF* have been explored including magnetic resonance imaging (MRI) [6], arterial spin labeling MRI [7], PET [8], Fick's lawbased optical systems [9], laser Doppler [10], diffuse correlation spectroscopy [11], and Doppler ultrasound [12], there remains a critical need for continuous, noninvasive instruments to measure *CBF* and *OC* in humans with intact skull. For example, the spatiotemporal resolution of PET is limited, and fMRI requires careful calibration of the scaling factor between the blood oxygen level dependent signal and the relative changes of de oxy hemoglobin concentration, as well as assumptions about the relationship between the changes in *CBF* and cerebral blood volume. Laser Doppler flow meter has limited penetration depth. Diffuse correlation spectroscopy has shown promising results, but it is still unclear whether it is practical enough to be used for continuous monitoring in humans. Fick's law-based systems are not entirely non invasive, since they require the injection of a chromophore, and therefore cannot be used for continuous monitoring.[13] Laser speckle contrast imaging method can effectively recover the *BF* and *OC* parameters. However, due to the cost and complexity, laser speckle imaging setups may not be readily available to researchers [2].

On the other hand, due to numerous advantages of low cost, portability, and non-ionizing radiation, near-infrared (NIR) diffuse optical spectroscopy (DOS) and tomography (DOT) have offered a promising alternative for continuous bedside monitoring of patients [14]. DOS and DOT have more than 30 year history of being used to access tissues total hemoglobin concentration, hemoglobin oxygen saturation, water and lipid concentration, tissue scattering, oxygen metabolism and blood flow [1,2,15-21]. NIR optical imaging modalities have shown a great potential to provide high spatiotemporal resolution and more quantitative imaging of hemodynamic responses [22]. In particular, dynamic optical imaging has allowed the exploration of time-resolved changes in tissues properties. The dynamics measured with DOT in the functional neuro imaging are due to the dynamics in blood volume and oxygenation in the scalp and brain. And the hemodynamics is caused by *CBF* and *OC* change associate with heart beat, vasomotion and vascular response to neuronal activity [23]. However, dynamic DOT imaging techniques provide only the change of total hemoglobin concentration (HbT) and oxygen saturation (SO_2), which cannot give the change of *CBF* and *OC* due to the hemodynamic response to neuronal activation. As such, new mathematical models connecting changes in *CBF* and *OC* to observed changes in *HbT* and SO_2 are required to guide more quantitative interpretation of neuron-activity. The model should be able to present indirect measurements of neuron-induced vascular parameters including blood flow (*BF*) and *OC*.

Developed mathematical models to reconstruct BF and OC of blood vessel and biological tissues

The technology now existing for obtaining quantitative information on how oxygen and blood are managed in the tissues is the principle of mass balance to the transport of oxygen in a blood vessel segment. [24] To model oxygen transport in a blood vessel by this principle, we consider a one-dimensional cylindrical vessel (blood vessel) with

***Corresponding author:** Zhen Yuan, Assistant Professor of Health Sciences, University of Macau, Av. Padre Tomás Pereira, Taipa, Macau, China, E-mail: yzhen.star@gmail.com

Received March 19, 2013; **Accepted** April 21, 2013; **Published** April 23, 2013

Citation: Yuan Z (2013) Model-Based Quantification of Blood Flow Rate and Oxygen Consumption Rate of Biological Tissues Using Image-Guided Near Infrared Light Spectroscopy. J Biosens Bioelectron 4: 135. doi:10.4172/2155-6210.1000135

R_i and R_o as the inner and outer radii, respectively, surrounded by the biological tissues. In addition, we assume all the oxygen (O_2) diffusing out the segment is consumed in a tissue region [25].

Mass balance in each segment for intravascular flux

The law of mass conservation stipulates that the amount of O_2 lost from a vascular segment must be equal to the diffuse O_2 flux to the tissues, determined by the perivascular oxygen gradients. For a steady case, we have

$$Q_{in}C_b[HbT]SO_{2,in} - Q_{out}C_b[HbT]SO_{2,out} = l_i\pi d_i J_i \quad (1)$$

in which Q_{in} (mL.s^{-1}) is the volumetric *BF* into the *ith* segment, Q_{out} the volumetric *BF* out the segment, d_i is the diameter of the *ith* segment, l_i the length of the *ith* segment, *HbT* the total hemoglobin concentration in the blood (moles), $SO_{2,in}$ the hemoglobin oxygen saturation flowing in the segment, $SO_{2,out}$ oxygen saturation flowing out of the segment, J_i the oxygen flux across the vessel wall (moles O_2 cm^{-2}.s^{-1}) and C_b is the oxygen binding capability of hemoglobin (C_b=1.39 mLO_2/gmHb; C_b=1. if the concentration of O_2 dissolved in plasma is considered) [25]. In addition, eq. (1) is rewritten in consideration of mean *BF*,

$$Q_iC_b[HbT](SO_{2,in} - SO_{2,out}) = l_i\pi d_i J_i \quad (2)$$

where Q_i is the mean *BF* in the *ith* segment. For a transient case, eq. (1) is further written

$$Q_{in}(t)C_b[HbT]SO_{2,in}(t) - Q_{out}(t)C_b[HbT]SO_{2,out}(t) - l_i\pi d_i J_i(t) = \frac{\partial M_{i,HbO_2}(t)}{\partial t} \quad (3)$$

in which M_{i,HbO_2} is the moles of oxygenated hemoglobin in the *ith* segment. According to the principle of mass balance, the third term on the left of Eq. (3) is actually the OC_i of the *ith* segment (mole O_2.s^{-1}). Considering the fact that each molecular of hemoglobin is able to carry four molecular oxygen, Eq. (3) is stated,

$$Q_{in}(t)C_b[HbT]SO_{2,in}(t) - Q_{out}(t)C_b[HbT]SO_{2,out}(t) - OC_i(t)/4 = \frac{\partial M_{i,HbO_2}(t)}{\partial t} \quad (4)$$

Mass balance in tissues based on global analysis for estimating intravascular flux

The oxygen consumed by the tissues (organs) is supplied from three blood vessels sources: capillaries, arterioles and venules. As such, mass balance for O_2 in the whole tissues (organ) yields for a steady case,

$$\sum_{i=1}^{M}(Q_{in}C_b[HbT]SO_{2,in} - Q_{out}C_b[HbT]SO_{2,out}) = \sum_{i=1}^{M} l_i\pi d_i J_i \quad (5)$$

and *M* is the number of blood vessels inside the tissues. Likewise, eq. (5) can be stated as if all the O_2 is consumed,

$$Q[HbT]_{blood}(SO_{2,ti} - SO_{2,to}) = OC/4 \quad (6)$$

For the dynamic case, eq. (6) is further written,

$$Q[HbT]_{blood}(SO_{2,ti} - SO_{2,to}) - OC/4 = \frac{\partial M_{HbO_2}}{\partial t} \quad (7)$$

where *Q* is the mean BF for all the blood vessels inside the tissues and is specified as the mean BF of tissues, $[HbT]_{blood}$ is the mean total blood hemoglobin concentration in the blood circulating through the tissues, *OC* is the mean oxygen consumption for the whole tissue volume V_{tissue}, M_{HbO_2} is the molar amount of oxygenated hemoglobin inside the measurement volume, and $SO_{2,ti}$, $SO_{2,to}$ is the averaged hemoglobin oxygen saturation at the inlet (artery) and outlet (vena) of the tissues, respectively. Moreover, it is noted that molar amount of oxygenated hemoglobin concentration of tissue is expressed as

$$M_{HbO_2} = SO_2[HbT]_{tissue}V_{tissue} = [HbO_2]V_{tissue} \quad (8)$$

Substituting Eq. (8) into (7), we obtain,

$$-\frac{OC}{4V_{tissue}} + \frac{Q}{V_{tissue}}[HbT]_{blood}(SO_{2,ti} - SO_{2,to}) = SO_2\frac{d[HbT]_{tissue}}{dt} + [HbT]_{tissue}\frac{dSO_2}{dt} = \frac{d[HbO_2]}{dt} \quad (9)$$

where V_{tissue} is the tissue volume and is assumed constant here, and SO_2 is the oxygen saturation of tissue. If the oxygen supply of tissues depends on the averaged oxygen saturation at the inlet and outlet of the tissues, tissue oxygen saturation should represent the weighted average of the arterial and venous saturation:

$$SO_2 = fSO_{2,ti} + (1-f)SO_{2,to} \quad (10)$$

Eq. (10) can be rewritten,

$$SO_{2,to} = (SO_2 - fSO_{2,ti})/(1-f) \quad (11)$$

Based on eq. (9) and (10), we get

$$\frac{dSO_2}{dt} = -\frac{OC}{4V_{tissue}[HbT]} + \frac{Q}{V_{tissue}[HbT]}[HbT]_{blood}\left(\frac{SO_{2,ti}}{1-f} - \frac{SO_2}{1-f}\right) - \frac{d[HbT]}{dt}\frac{SO_2}{[HbT]} \quad (12)$$

Eq. (12) is the developed mathematical model that connects changes in *BF* and *OC* to known HbT and SO_2 captured by DOT. As such, mean *OC* and *BF* can be recovered by fitting eq. (12) to time-resolved tissues oxygenation measurements. Eq. (12) is an ordinary partial differential equation that can be solved iteratively by Runge-Kutta 4th order method coupled with finite element method [26,27]. The fitting method is described as follows: with any given initial values for *OC* and *BF* within the specified range, this scheme is to optimize the *OC* and *BF* parameters based on the solution of eq. (12) to reach the minimized objective function in eq. (13).

$$\text{Min: } \boldsymbol{F} = \sum_{i=1}^{M}\left(SO_{2i}^{m} - SO_{2i}^{c}\right)2 \quad (13)$$

in which SO_{2i}^{m} is the measured oxygenation parameter from M discrete time points, SO_{2i}^{c} is calculated oxygenation parameter from Eq. (12) for the same time points. Note the *BF* and *OC* are assumed constant during the measurements for the specified time range, due to the need for a sufficient time interval to obtain stable fitting results. Finally, it should point out that Carp et al. also used a very similar model as eq. (12) to analyze the dynamics response of compressed breast tissues though it seem that their model has no strong theoretical basis [28].

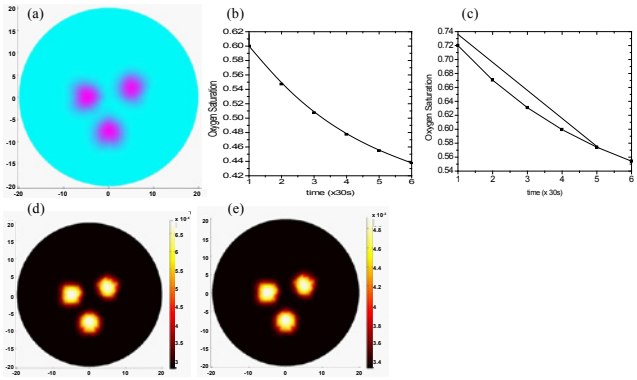

Figure 1: Test geometry: (a) Generated simulated oxygenation measurement using eq. (12); (b) for the background; (c) targets; (d) Recovered *BF* image and (e) *OC* image.

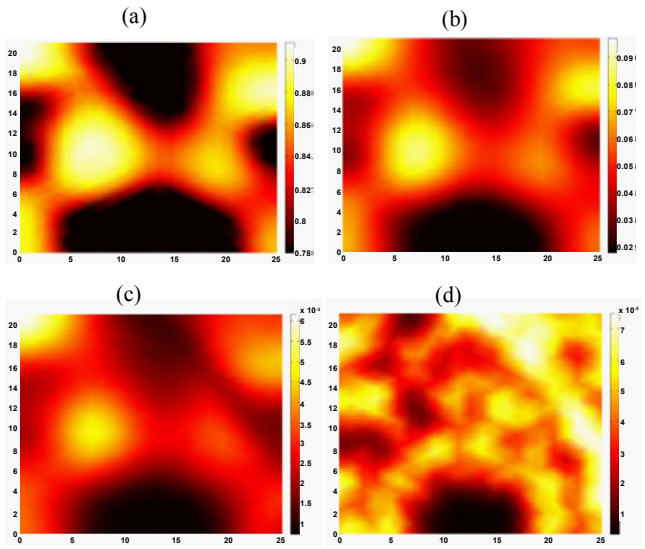

Figure 2: Reconstructed (a) SO_2; (b) *HbT* (mM); (c) volume normalized *BF* (ml/ml/s) and (d) volume normalized *OC* (μmol/ml/s) images after 1 minute.

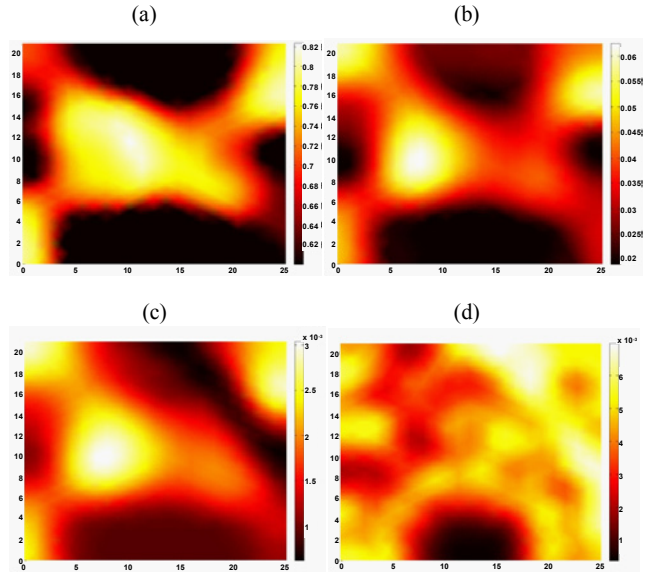

Figure 3: Reconstructed (a) SO_2, (b) *HbT* (mM), (c) volume normalized *BF* (ml/ml/s), and (d) volume normalized *OC* (μmol/ml/s) images after 2 minutes.

Results and Discussion

In this section, we show reconstruction results that demonstrate feasibility of the recovery of mean *BF* and *OC* based on the developed model described above. The fitting algorithm is evaluated using simulation test and small animal experiments.

Simulations are first conducted to validate the merits of the developed reconstruction algorithm for recovery *BF* and *OC*. For the test geometry, a circular background region (20 mm in radius) contains three circular targets (2 mm in radius each) positioned at 2 (top right), 9 (top left) and 6 o'clock (bottom), as displayed in figure 1a. The volume normalized BF (BF/V_{tissue}) and *OC* (OC/V_{tissue}) for the background media is 2.73×10^{-4} mL/mL/s and 3.283×10^{-3} µmol/mL/s, respectively, while the three inclusions have *OC* of 4.925×10^{-3} µmol/mL/s and BF of 6.825×10^{-4} mL/mL/s. The simulated oxygenation saturation signals were generated using eq. (12) with 2% random Gaussian noise added. The initial parameters are given by: HbT_{blood}=0.72 mM, f=0.2, $SO_{2,ti}$=0.98,[27] HbT_{target}=0.12 mM, $HbT_{background}$=0.06 mM. The change of simulated oxygen saturation vs time is given in figures 1b and 1c for background media and the targets, respectively. The recovered *BF* and *OC* are shown in figures 1d and 1c, respectively.

It is observed in figure 1 that targets and background media are effectively recovered according to the position, size and quantitative *BF* and *OC*.

Animal experiments were performed using a dynamic DOT

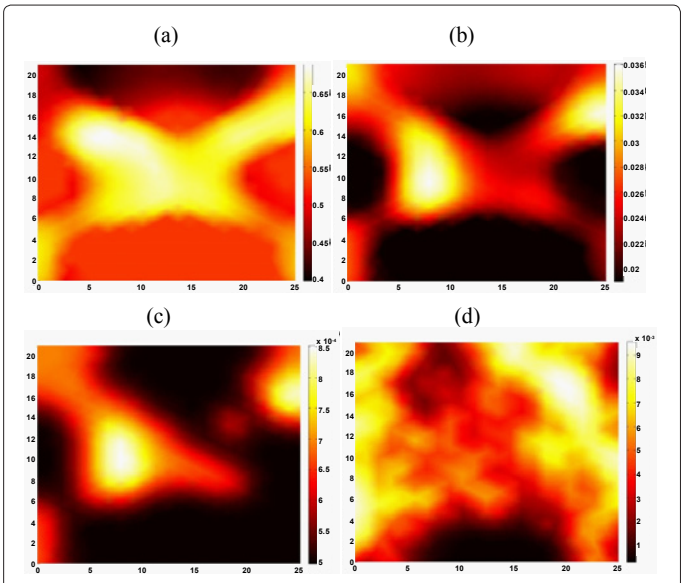

Figure 4: Reconstructed (a) SO_2, (b) *HbT* (mM), (c) volume normalized *BF* (ml/ml/s) and (d) volume normalized *OC* (μmol/ml/s) images after 4 minutes.

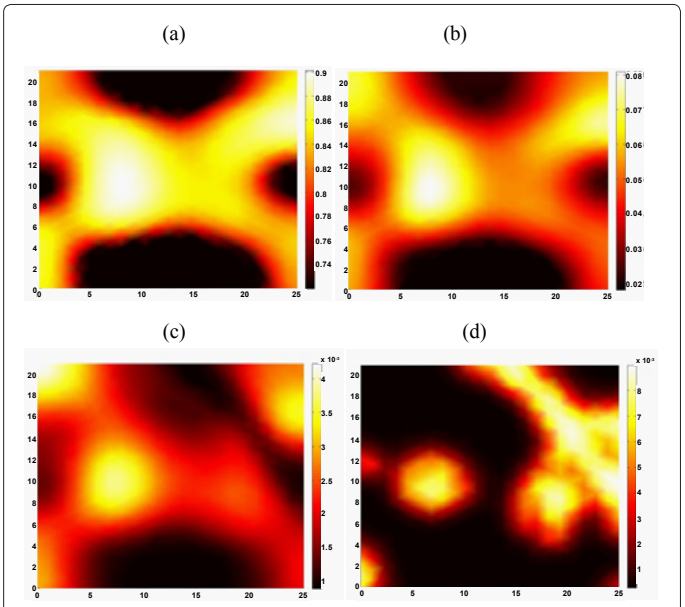

Figure 5: Reconstructed (a) SO_2, (b) *HbT* (mM), (c) volume normalized *BF* (ml/ml/s) and (d) volume normalized *OC* (μmol/ml/s) images after 6 minutes.

imaging system that has been described in detail elsewhere [29]. To reconstruct *BF* and *OC*, the initial parameters are given by: HbT_{blood}=0.72 mM, f=0.2, $SO_{2,ti}$=0.98. The dynamic *HbT* and SO_2 parameters are first calculated by fitted the reconstructed optical absorption coefficient using Beer's law at wavelengths 633 nm, 760 and 853 [29]. In addition, due to high nonlinear distribution of dynamic SO_2, the SO_2 distribution curve is then separated into several approximated linear segments to improve the fitting accuracy of *BF* and *OC*. Then mean *BF* and *OC* are fitted for each linear segment based on different initial values of HbT and SO_2. In this investigation, there are 6 measurements at time 1, 2, 4, 6, 8 and 25 minutes. For each segment, only 2 two discrete oxygenation measurements are used for the fitting calculation. And we specify the fitted mean *BF* and *OC* for each segment as the values at the stating point of the segment. For example, we name the mean *BF* and *OC* fitted between time 1 and 2 minutes as the *BF* and *OC* at 1 minute.

Figures 2-6 present the reconstructed *in vivo HbT*, SO_2, volume normalized *BF* and *OC* images. We see that the seizure is remarkably imaged with the highest contrast in *HbT*, SO_2, volume normalized *BF*. In addition, the *OC* image is not effectively recovered due to insufficient time interval to obtain stable fitting results. Further, it is observed from the peak values of *BF* shown in figure 7 that the recovered blood flow values (3.9-36.9 ml/100 ml/min) are in good agreement with reported *CBF* of rats (between 10-120 ml/100ml/min) and human being (20-160 ml/100 ml/min) [30,31]. The *in vivo* results shown here further validate the merits of the developed mathematical model.

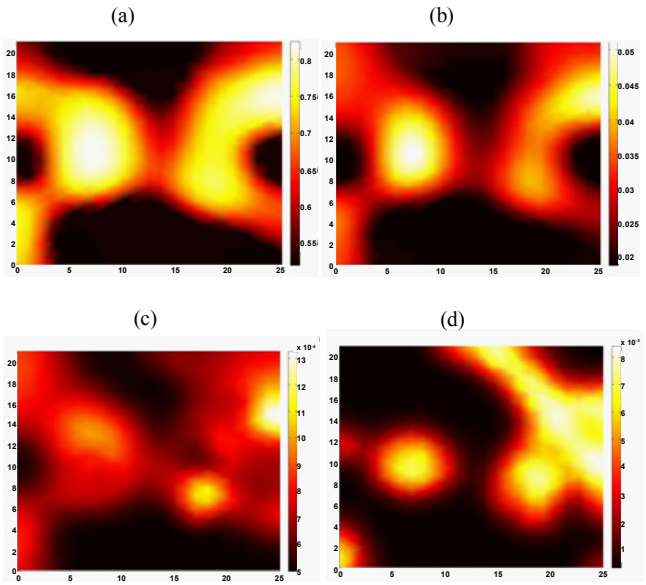

Figure 6: Reconstructed (a) SO_2, (b) *HbT* (mM), (c) volume normalized *BF* (ml/ml/s) and (d) volume normalized *OC* (μmol/ml/s) images after 8 minutes.

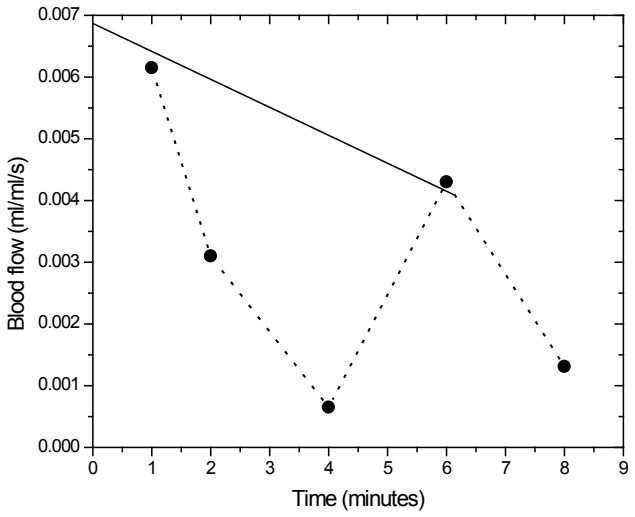

Figure 7: Distribution of peak values of blood flow for seizure at different time.

In summary, we have developed an effective model that is capable to estimate the *OC* and *BF* of biological tissues. However, this model can only provide mean vales of *BF* and *OC* during a time interval. And more measurements are required for this time interval to obtain stable and accurate fitting results. Our simulations and *in vivo* tests indicate at least 3 or 4 measurements for this time interval are needed to achieve reliable fitting computation of both *BF* and *OC*. In addition, highly nonlinear change of oxygen saturation during the time interval should be avoided to ensure the efficacy of the developed model. Ultimately, the assumption and utilization of constant tissues volume and other known tissues parameters will also affect the accuracy of the fitting calculation. In future, we plan to combine the laser speckle imaging setups with multiple wavelengths DOT imaging systems to quantitatively measure and image *BF* and *OC* of a local blood vessel network [2]. Consequently, the developed imaging systems will enable us to accurately and quantitatively estimate the *BF* and *OC* of biological tissues based on the captured physiological parameters of tissues and vascular parameters from blood segments as well as the developed model.

References

1. Durduran T, Yu G, Burnett MG, Detre JA, Greenberg JH, et al. (2004) Diffuse optical measurement of blood flow, blood oxygenation, and metabolism in a human brain during sensorimotor cortex activation. Opt Lett 29: 1766-1768.
2. Dunn AK, Devor A, Bolay H, Andermann ML, Moskowitz MA, et al. (2003) Simultaneous imaging of total cerebral hemoglobin concentration, oxygenation, and blood flow during functional activation. Opt Lett 28: 28-30.
3. Lauritzen M (2001) Relationship of spikes, synaptic activity, and local changes of cerebral blood flow. J Cereb Blood Flow Metab 21: 1367-1383.
4. Logothetis NK, Pauls J, Augath M, Trinath T, Oeltermann A (2001) Neurophysiological investigation of the basics of the fMRI signal. Nature 412: 150-157.
5. Sakadzić S, Yuan S, Dilekoz E, Ruvinskaya S, Vinogradov SA, et al. (2009) Simultaneous imaging of cerebral partial pressure of oxygen and blood flow during functional activation and cortical spreading depression. Appl Opt 48: D169-D177.
6. Logothetis NK (2008) What we can do and what we cannot do with fMRI. Nature 453: 869-878.
7. Williams DS, Detre JA, Leigh JS, Koretsky AP (1992) Magnetic resonance imaging of perfusion using spin inversion of arterial water. Proc Natl Acad Sci U S A 89: 212-216.
8. Mintun MA, Raichle ME, Martin WR, Herscovitch P (1984) Brain oxygen utilization measured with O-15 radiotracers and positron emission tomography. J Nucl Med 25: 177-187.
9. Patel J, Marks K, Roberts I, Azzopardi D, Edwards AD (1998) Measurement of cerebral blood flow in newborn infants using near infrared spectroscopy with indocyanine green. Pediatr Res 43: 34-39.
10. Fabricius M, Akgören N, Dirnagl U, Lauritzen M (1997) Laminar analysis of cerebral blood flow in cortex of rats by laser-Doppler flowmetry: a pilot study. J Cereb Blood Flow Metab 17: 1326-1336.
11. Cheung C, Culver JP, Takahashi K, Greenberg JH, Yodh AG (2001) *In vivo* cerebrovascular measurement combining diffuse near-infrared absorption and correlation spectroscopies. Phys Med Biol 46: 2053-2065.
12. Kirkham FJ, Padayachee TS, Parsons S, Seargeant LS, House FR, et al. (1986)

Transcranial measurement of blood velocities in the basal cerebral arteries using pulsed Doppler ultrasound: velocity as an index of flow. Ultrasound Med Biol 12: 15-21.

13. Themelis G, D'Arceuil H, Diamond SG, Thaker S, Huppert TJ, et al. (2007) Near-infrared spectroscopy measurement of the pulsatile component of cerebral blood flow and volume from arterial oscillations. J Biomed Opt 12: 014033.
14. Tromberg BJ, Pogue BW, Paulsen KD, Yodh AG, Boas DA, et al. (2008) Assessing the future of diffuse optical imaging technologies for breast cancer management. Med Phys 35: 2443-2451.
15. Zhou C, Choe R, Shah N, Durduran T, Yu G, et al. (2007) Diffuse optical monitoring of blood flow and oxygenation in human breast cancer during early stages of neoadjuvant chemotherapy. J Biomed Opt 12: 051903.
16. Ntziachristos V, Yodh AG, Schnall MD, Chance B (2002) MRI-guided diffuse optical spectroscopy of malignant and benign breast lesions. Neoplasia 4: 347-354.
17. Hillman EM (2007) Optical brain imaging in vivo: techniques and applications from animal to man. J Biomed Opt 12: 051402.
18. Brooksby B, Jiang S, Dehghani H, Pogue BW, Pausen KD, et al. (2005) Combining near-infrared tomography and magnetic resonance imaging to study *in vivo* breast tissues: implementation of a Laplacian-type regularization to incorporate magnetic resonance structure. J Biomed Opt 10: 011504.
19. Hielscher AH, Klose AD, Scheel AK, Moa-Anderson B, Backhaus M, et al. (2004) Sagittal laser optical tomography for imaging of rheumatoid finger joints. Phys Med Biol 49: 1147-1163.
20. Yuan Z, Zhang Q, Sobel E, Jiang H (2007) Three-dimensional diffuse optical tomography of osteoarthritis: initial results in the finger joints. J Biomed Opt 12: 034001.
21. Hebden JC, Yates TD, Gibson A, Everdell N, Arridge SR, et al. (2005) Monitoring recovery after laser surgery of the breast with optical tomography: a case study. Appl Opt 44: 1898-1904.
22. Strangman G, Boas DA, Sutton JP (2002) Non-invasive neuroimaging using near-infrared light. Biol Psychiatry 52: 679-693.
23. Toronov V, Franceschini MA, Filiaci M, Fantini S, Wolf M, et al. (2000) Near-infrared study of fluctuations in cerebral hemodynamics during rest and motor stimulation: temporal analysis and spatial mapping. Med Phys 27: 801-815.
24. Tsai AG, Johnson PC, Intaglietta M (2003) Oxygen gradients in the microcirculation. Physiol Rev 83: 933-963.
25. Sharan M, Vovenko EP, Vadapalli A, Popel AS, Pittman RN (2008) Experimental and theoretical studies of oxygen gradients in rat pial microvessels. J Cereb Blood Flow Metab 28: 1597-1604.
26. Michael M, William HP, Saul AT, William TV, Brian PF (1986-1992) Numerical Recipes in Fortran 77. Cambridge University Press.
27. Yuan Z, Jiang H (2012) A calibration-free, one-step method for quantitative photoacoustic tomography. Med Phys 39: 6895-6899.
28. Carp SA, Selb J, Fang Q, Moore R, Kopans DB, et al. (2008) Dynamic functional and mechanical response of breast tissue to compression. Opt Express 16: 16064-16078.
29. Wang Q, Liang X, Liu Z, Zhang Q, Carney P, et al. (2008) Visualizing localized dynamic changes during epileptic seizure onset *in vivo* with diffuse optical tomography. Med Phys 35: 216-224.
30. Hernández MJ, Brennan RW, Bowman GS (1978) Cerebral blood flow autoregulation in the rat. Stroke 9: 150-154.
31. Sharples PM, Stuart AG, Matthews DS, Aynsley-Green A, Eyre JA (1995) Cerebral blood flow and metabolism in children with severe head injury. Part 1: Relation to age, Glasgow coma score, outcome, intracranial pressure, and time after injury. J Neurol Neurosurg Psychiatry 58: 145-152.